Astronomy & Astrophysics manuscript no. ges˙extinction˙accepted
February 12, 2015

The Gaia-ESO Survey: Tracing interstellar extinction*

M. Schultheis[1], G. Kordopatis[2,3], A. Recio-Blanco[1], P. de Laverny[1], V. Hill[1], G. Gilmore[3], E. J. Alfaro[4], M.T. Costado[4], T. Bensby[5], F. Damiani[6], S. Feltzing[5], E. Flaccomio[6], C. Lardo[7], P. Jofre[3], L. Prisinzano[6], S. Zaggia[8], F. Jimenez-Esteban[9,10], L. Morbidelli[11], A.C. Lanzafame[12], A. Hourihane[3], C. Worley[3], and P. Francois[13]

[1] Université de Nice Sophia-Antipolis, CNRS, Observatoire de Côte d'Azur, Laboratoire Lagrange, 06304 Nice Cedex 4, France
e-mail: mathias.schultheis@oca.eu
[2] Leibniz-Institut für Astrophysik Potsdam (AIP), An der Sternwarte 16, 14482 Potsdam, Germany
[3] Institute of Astronomy, University of Cambridge, Madingley Road, CB3 0HA, United KIngdom
[4] Instituto de Astrofísica de Andalucía-CSIC, Apdo. 3004, 18080 Granada, Spain
[5] Lund Observatory, Department of Astronomy and Theoretical Physics, Box 43, SE-221 00 Lund, Sweden
[6] INAF - Osservatorio Astronomico di Palermo, Piazza del Parlamento 1, 90134, Palermo, Italy
[7] Astrophysics Research Institute, Liverpool John Moores University, 146 Brownlow Hill, Liverpool L3 5RF, United Kingdom
[8] INAF - Padova Observatory, Vicolo dell'Osservatorio 5, 35122 Padova, Italy
[9] Centro de Astrobiología (INTA-CSIC), Departamento de Astrofísica, PO Box 78, E-28691, Villanueva de la Cañada, Madrid, Spain
[10] Suffolk University, Madrid Campus, C/ Valle de la Via 3, 28003, Madrid, Spain
[11] INAF - Osservatorio Astrofisico di Arcetri, Largo E. Fermi 5, 50125, Florence, Italy
[12] Dipartimento di Fisica e Astronomia, Sezione Astrofisica, Universitá di Catania, via S. Sofia 78, 95123, Catania, Italy
[13] GEPI, Observatoire de Paris, CNRS, Université Paris Diderot, 5 Place Jules Janssen, 92190 Meudon, France

Preprint online version: February 12, 2015

ABSTRACT

Context. Large spectroscopic surveys have enabled in the recent years the computation of three-dimensional interstellar extinction maps thanks to accurate stellar atmospheric parameters and line-of-sight distances. Such maps are complementary to 3D maps extracted from photometry, allowing a more thorough study of the dust properties.

Aims. Our goal is to use the high-resolution spectroscopic survey Gaia-ESO in order to obtain with a good distance resolution the interstellar extinction and its dependency as a function of the environment and the Galactocentric position.

Methods. We use the stellar atmospheric parameters of more than 5000 stars, obtained from the Gaia-ESO survey second internal data release, and combine them with optical (SDSS) and near-infrared (VISTA) photometry as well as different sets of theoretical stellar isochrones, in order to calculate line-of-sight extinction and distances. The extinction coefficients are then compared with the literature to discuss their dependancy on the stellar parameters and position in the Galaxy.

Results. Within the errors of our method, our work does not show that there is any dependence of the interstellar extinction coefficient on the atmospheric parameters of the stars. We do not find any evidence of the variation of $E(J-H)/E(J-K)$ with the angle from the Galactic centre nor with Galactocentric distance. This suggests that we are dealing with a uniform extinction law in the SDSS $ugriz$ bands and the near-IR $JHKs$ bands. Therefore, extinction maps using mean colour-excesses and assuming a constant extinction coefficient can be used without introducing any systematic errors.

Key words. Galaxy: structure, stellar content – ISM: dust, extinction

1. Introduction

Understanding the dust spatial distribution in the Milky is a crucial part of Galactic archeology. Indeed, it can reveal important features of Galaxy evolution, such as the location and intensity of past star formation episodes (Boulanger 2007). Among the literature, the most commonly used full-sky dust map is that of Schlegel et al. (1998) obtained with COBE/DIRBE data, later improved by Schlafly et al. (2010) and Schlafly & Finkbeiner (2011) by adding correction terms mainly due to the adopted reddening law. Other 2-D extinction maps result from specific stellar populations. For example, red clump stars are considered to be an ideal tracer for extinction as their mean intrinsic colour varies only slightly with metallicity therefore making them a reliable tracer of dust extinction (see for example Gonzalez et al. 2011, 2012; Nataf et al. 2013). However, such studies require a sufficient number of red clump stars in order to have a good spatial coverage and hence are limited to regions with high stellar density (close to the plane or towards the Bulge). On the other hand, Nidever et al. (2012) mapped the extinction with the so-called Rayleigh Jeans Colour Excess method (RJCE) which is based on a combination of near and mid-infrared photometry (e.g. H and [4.5]). RJCE determines 2D star-by-star reddening at high-resolution ($2 \times 2'$) allowing to penetrate the heavily obscured Galactic mid-plane.

The recent growth of large surveys together with the increasing volume of data has pushed forward the extinction mapping and allowed to trace its distribution in three dimensions. The first of these 3D extinction models was constructed by Drimmel et al. (2003), by fitting the far and near-IR data from the COBE/DIRBE instrument. Marshall et al. (2006) used the

* Based on observations collected with the FLAMES spectrograph at the VLT/UT2 telescope (Paranal Observatory, ESO, Chile), for the Gaia-ESO Large Public Survey, programme 188.B-300

2MASS colours together with the stellar population synthesis model of Besançon (Robin et al. 2003) to trace extinction in 3D for the Galactic Bulge region ($|l| < 90, |b| < 10$) with a spatial resolution of 15′.

A number of photometric techniques have been used to study the dust in 3D (Green et al. 2014,Schlafly et al. 2014, Bailer-Jones 2011, Hanson & Bailer-Jones 2014, Sale 2012, Sale et al. 2014, Lallement et al. 2014). Chen et al. (2014a) traced the stellar locus similar as done by Berry et al. (2012) method by combining optical, 2MASS and WISE photometry and defining the reference stellar locus as well as fixing the extinction law. Their map covers about 6000. sq. degree with a small overlap to some of our GES fields (see Sect. 5)

Until now, most of the interstellar extinction studies were done mainly by photometric techniques. The already available or upcoming large spectroscopic surveys (RAVE, APOGEE, Gaia-ESO , GALAH, 4MOST, etc..) provide an important quantity of accurate stellar parameters of different stellar populations. It is therefore possible to probe the 3D distribution of interstellar dust using the expected colours of the targets and comparing them with the observed ones. The Gaia space mission of ESA will provide in the following years two-dimensional maps for most of the Galaxy but also individual extinction estimates together with measured parallaxes (see Bailer-Jones et al. 2013 for more details). In this paper we will use stellar properties derived from the Gaia-ESO survey (GES, Gilmore et al. 2012) to probe the interstellar extinction in three dimensions as done by Schultheis et al. (2014b) using APOGEE data. They compared 3D extinction models in the Galactic Bulge region with Marshall et al. (2006) and Schultheis et al. (2014a) and found a steep rise in extinction in the first few kpc and a flattening of the extinction at about 4 kpc from the Sun. While Schultheis et al. (2014b) and Wang & Jiang (2014) probed the interstellar dust properties with APOGEE in the Galactic plane ($|z| < 1$ kpc), the GES fields are located at much higher Galactic latitudes ($|b| > 20^o$). The GES data are thus complementary to APOGEE allowing to trace the dust extinction at higher Galactic height |z| and compare them with available 3D dust models. In Sect. 2, we describe the sample of stars that has been used, in Sect 3 we present the method employed in the determination of the extinction and the distances. In Sections 4 and 5, we compare and discuss the extinctions to existing 2D and 3D maps, and we finish in Sect. 6 with the discussion about the universality of the extinction law.

2. The sample

The Gaia-ESO survey (GES) is a public spectroscopic survey targeting $\sim 10^5$ stars, covering all the major components of the Milky Way, from the halo to star forming regions, with the purpose of characterising the chemistry and kinematics of these populations. It uses the FLAMES multi-object spectrograph on the VLT UT2 telescope to obtain high quality, uniformly calibrated spectra. The GES processing flow goes from target selection, through data reduction, spectrum analysis, astrophysical parameter determination, calibration and homogenisation. A detailed description of the data processing cascade and general characterisation of the data set can be found in Gilmore et al. (2015, in prep.), In this paper, we analyse the second data release (DR2) GES results for ~ 10 000 Milky Way stars observed with the high-resolution gratings HR10 centred at 5488 Å (R ~ 19800) and HR21 centred at 8757 Å (R ~ 16200) of the GIRAFFE spectrograph. All the targets were selected from VISTA photometry, with colour cuts in the range $0.2 < (J-K) < 0.8$, and magnitude cuts between $12.5 < J < 17.5$ (c.f. Gilmore et al. 2012). Additional SDSS photometry is also available which we will use in this work. Considerable effort has been invested in the determination of the stellar parameters. The stellar parameters have been derived from three different methods, MATISSE (Recio-Blanco et al. 2006), SME (Valenti & Piskunov 1996) and FERRE (Allende Prieto et al. 2006). This ensures a reliable determination of the derived stellar parameters, a crucial step to get accurate stellar abundances and line-of-sight distances. The homogenisation of the results from the three nodes which was verified during the GES parameters validation process leads to the so-called “Recommended stellar parameters”. For our analysis we used those parameters, i.e. effective temperature (T_{eff}), surface gravities ($\log g$), global metallicities ([M/H]) and α-elements ([α/Fe]). The relative error distributions peak at 70 K for T_{eff}, 0.10 dex for $\log g$, 0.08 dex for [M/H] and 0.03 dex for [α/Fe]. More details about the related GES parameterisation pipeline can be found in Recio-Blanco et al. (2014a).

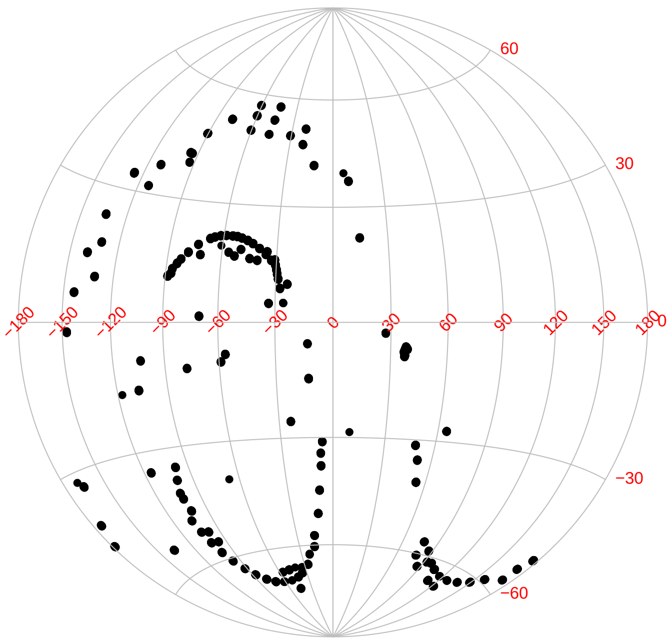

Fig. 1. Field centres of the GES-DR2 fields in Galactic coordinates

To achieve the scope of this paper, we selected targets with available photometry from the VISTA Variables in the Via Lactea (VVV) survey (Minniti et al. 2010) or 2MASS, together with reliable atmospheric parameters obtained from spectroscopy. This implied that we selected only the targets with spectra having a signal-to-noise $S/N > 10$, errors in radial velocity $\sigma(RV) < 1.5 \mathrm{km\,s^{-1}}$, and low internal dispersion on T_{eff} and $\log g$ between the three different nodes (see Sect. 3). The first two criteria ensure that the random errors of the algorithms are minimised, and the ($\sigma_{T_{eff}}, \sigma_{\log g}$) criterium ensures a minimisation of the internal errors of the GES homogenisation pipeline. Our sample consists thus of 5603 stars with only Near-IR photometry, while 1106 stars have ugrizJHK photometry.

Figure 1 shows the field centres of the GES-DR2 fields in Galactic coordinates.

3. Distance and extinction determination

The routine that has been used to determine the absolute magnitudes of the stars in different photometric bands (and from that the extinctions and the distances), is based on the one described in Kordopatis et al. (2011b), and already successfully applied in Gazzano et al. (2013); Kordopatis et al. (2013); Recio-Blanco et al. (2014b). Briefly, the method projects the measured atmospheric parameters ($\hat{\theta} \equiv \mathrm{T_{eff}}, \log \mathrm{g}, [\mathrm{M/H}]$) and colours on a given set of theoretical isochrones. The set of isochrones used is defined for a given age a and a range of iron abundances [Fe/H] within the [M/H] error bars. For this paper, we assume that the [Fe/H] values of the isochrones are similar enough to [M/H], to use the approximation [Fe/H]=[M/H] while performing the projection on the isochrones. According to Recio-Blanco et al. (in prep), this is true for most of the stars in the GES iDR2.

The probability density function for a given star, $W(a, m, [\mathrm{Fe/H}])$, is defined as:

$$W(a, m, [\mathrm{Fe/H}]) = dm \cdot \exp\left(- \sum_i \frac{(\theta_i - \hat{\theta}_i)^2}{2\sigma^2_{\hat{\theta}_i}} \right) \quad (1)$$

where θ_i is the theoretical $\mathrm{T_{eff}}$, $\log g$ or [Fe/H], $\hat{\theta}_i$ and $\sigma_{\hat{\theta}_i}$ are the measured parameters and their respective errors, and dm is the mass step between two points of the same isochrone, introduced in order to impose a uniform prior on the stellar mass. We note that Zwitter et al. (2010) have shown that having such a flat prior on mass does not affect significantly the final derived distances, when compared to the use of a combination of a more realistic mass function (e.g. Chabrier 2003) with a luminosity prior on the surveyed stars (see, Zwitter et al. 2010, their Sect. 2.2, for more details).

The expected value of the absolute magnitude M_τ in a given photometric band τ of a given star is then obtained by computing the weighted mean:

$$M_\tau = \frac{\sum_{a,m,[\mathrm{Fe/H}]} W(a, m, [\mathrm{Fe/H}]) \cdot M_\tau(a, m, [\mathrm{Fe/H}])}{\sum_{a,m,[\mathrm{Fe/H}]} W(a, m, [\mathrm{Fe/H}])}, \quad (2)$$

where $\sum_{a,m,[\mathrm{Fe/H}]}$ is the triple sum over the ages, masses and iron abundances. The associated variance of the expected absolute magnitude M_τ is obtained by:

$$\sigma^2(M_\tau) = \frac{\sum_{a,m,[\mathrm{Fe/H}]} W(a, m, [\mathrm{Fe/H}]) \cdot [M_\tau - M_\tau(a, m, [\mathrm{Fe/H}])]^2}{\sum_{a,m,[\mathrm{Fe/H}]} W(a, m, [\mathrm{Fe/H}])}. \quad (3)$$

We have used two sets of isochrones: the Yonsei-Yale ones (Demarque et al. 2004) with the Lejeune et al. (1998) colour tables, and the Padova ones (Marigo 1998; Bressan et al. 2012). The Yonsei-Yale (YY) isochrones have been computed using the provided interpolation code of YY, from which we generated a set of isochrones with a constant step in age of 1 Gyr, starting from 1 Gyr to 14 Gyr, therefore resulting to flat prior on the age of the stars. As far as the metallicities are concerned, they are within a range of $-3 < [\mathrm{Fe/H}] < 0.8$ dex, constantly spaced by 0.1 dex. The $\alpha-$enhancements of the isochrones have been selected in the following way:

- $[\mathrm{Fe/H}] \geq 0$ dex, then $[\alpha/\mathrm{Fe}] = 0.0$ dex
- $-0.3 \leq [\mathrm{Fe/H}] \leq -0.1$ dex, then $[\alpha/\mathrm{Fe}] = +0.1$ dex
- $-0.6 \leq [\mathrm{Fe/H}] \leq -0.4$ dex, then $[\alpha/\mathrm{Fe}] = +0.2$ dex
- $-0.9 \leq [\mathrm{Fe/H}] \leq -0.7$ dex, then $[\alpha/\mathrm{Fe}] = +0.3$ dex
- $[\mathrm{Fe/H}] \leq -1$ dex, then $[\alpha/\mathrm{Fe}] = +0.4$ dex

Table 1. Median errors in distance when adding an offset to the derived atmospheric parameters for giants (log g < 3) and dwarfs and subgiants (log g > 3). The "+" sign specifies adding the offset, the "-" sign subtracting the offset

	$\mathrm{T_{eff}} \pm 100$ K %	$\log g \pm 0.2$ dex %	[M/H] $\pm$ 0.1 dex %
Giants (+)	1.1	19.7	1.8
Giants (-)	5.1	34.3	1.3
Dwarfs (+)	5	2.9	7.6
Dwarfs (-)	11	8.1	9.7

According to Carpenter et al. (2001), the $(JK)_{ESO}$ provided by the Yonsei-Yale isochrones match very well the $(JK_s)_{2MASS}$ and $(JK_s)_{VHS}$, so no colour transformation is needed when manipulating the magnitudes from the different photometric systems.

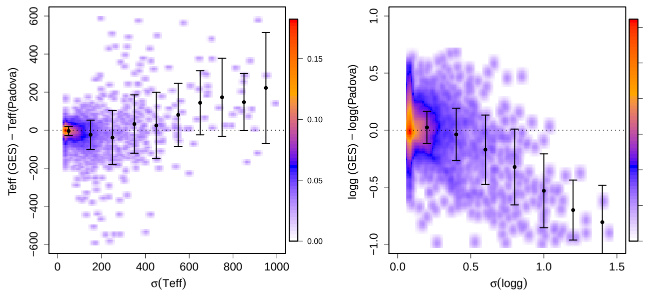

Fig. 2. Left: Density plot of the difference between $\mathrm{T_{eff}}$ and the corresponding temperature from the isochrones and the dispersion of $\mathrm{T_{eff}}$ between the three nodes (see text). The black points indicate the mean (in 100 K steps) and the error bars the standard deviations. **Right:** The same but for $\log g$. The black points indicate the mean (in 0.2 dex steps) and the error-bars the standard deviations.

As far as the Padova isochrones are concerned, they have been downloaded using the online interpolation interface[1] which allows us to select the output photometric system (2MASS, SDSS, VISTA). The considered metallicity range is smaller than the one of YY (from −2.2 dex to +0.2 dex in steps of 0.1 dex with solar-scale $\alpha-$abundances), computed with steps in age of 0.5 Gyr.

Once the absolute magnitudes are computed, the colours are derived and the colour excess are deduced by subtracting the theoretical colour from the observed one in the five SDSS and 3 VISTA filters. The colour excess derived using this method is hereafter referred to as $\mathrm{E}_{\lambda_1-\lambda_2}$ with $\lambda = u, g, r, i, z, J, H, K_s$. About 5% of our stars show negative extinction, most of which are fainter than $\mathrm{K_s} > 14.5$. We omitted those from our analysis. The distances were calculated using the usual relation :

$$\log_{10} d = \frac{K_s - M_{K_s} - A(K_s) + 5}{5} \quad (4)$$

with d expressed in pc, and adopting $\mathrm{A(K_s)} = 0.528 \times \mathrm{E(J - K_s)}$ (Nishiyama et al. 2009) similar to what has been done in Schultheis et al. (2014b). The errors in the derived distances include errors in $\mathrm{T_{eff}}$, $\log g$ and [M/H] and errors on the apparent magnitude J and $\mathrm{K_s}$ as well as the extinction $\mathrm{A_{K_s}}$. For more

[1] http://stev.oapd.inaf.it/cgi-bin/cmd

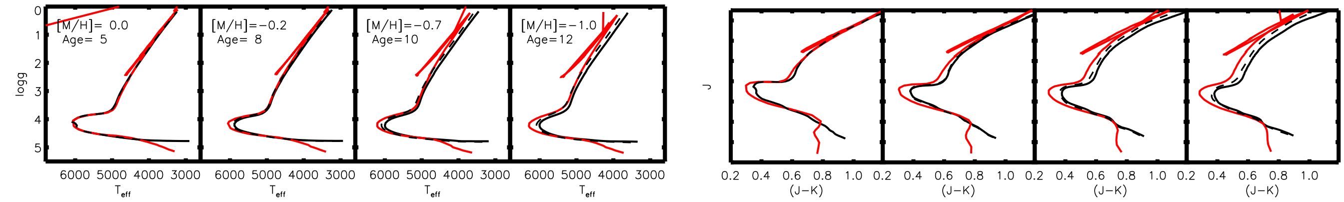

Fig. 3. Left: Isochrones in the $T_{\rm eff}$ vs. log g space for different combinations of [M/H] and ages. The red line shows the Padova isochrones. The dashed black line indicates the Yonsei-Yale isochrones without α-elements while the plain black line is for YY models with alpha enhancement. **Right:** Similar as in the left panel but in the J–K vs. K colour-magnitude diagram

details, we refer to Kordopatis et al. (2011a). Other than the internal errors in the stellar parameters, the absolute calibration in $T_{\rm eff}$, log g and [Fe/H] is also crucial for the errors in our derived distances.

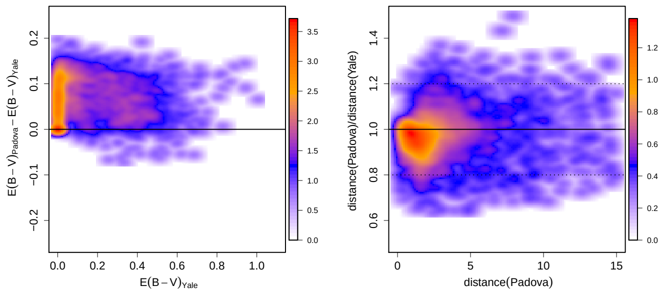

Fig. 4. Left: Density distribution of the difference in E(B-V) derived from the Padova and the Yonsei-Yale (YY) isochrones as a function of E(B-V) from the YY isochrones. **Right:** Ratio of distances derived from the Padova isochrones to the YY stellar library, as a function of distance. The dashed horizontal lines indicate ±20% difference.

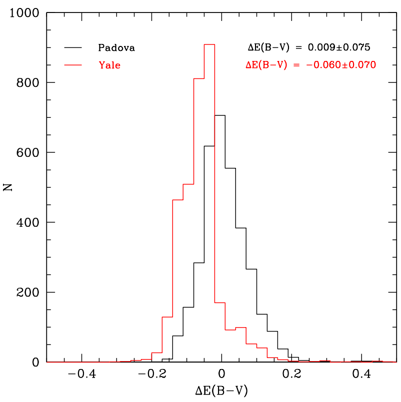

Fig. 5. Histogram of the differences between our derived E(B-V) and the Schlegel SFD98 value for high galactic latitude stars (|b| > 10°).The black line are the derived extinction values using the Padova isochrones, the red line those from the Yale isochrones. The mean value and the r.m.s scatter is indicated on the top left corner.

Table 1 shows the errors in the derived distances (in %) if one assumes an offset in $T_{\rm eff}$ ± 100 K, log g ± 0.2 dex and [M/H] ± 0.1 dex. Clearly seen is the large impact of log g for giants with up to ∼ 34% error in the derived distances while temperature and metallicity offsets play only a minor role. For dwarf stars and subgiants, the effect of the surface gravity is the smallest (< 10%) due to the fact the main-sequences roughly overlap at all ages. On the other hand, offsets in $T_{\rm eff}$ have a larger effect for dwarf stars, because of the overall steeper slope of the main-

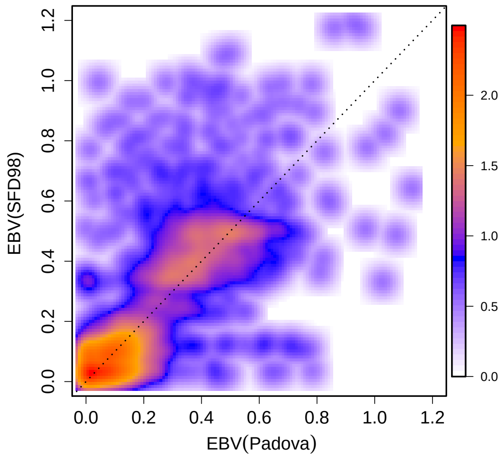

Fig. 6. Density plot of E(B-V) against E(B-V) from SFD98.

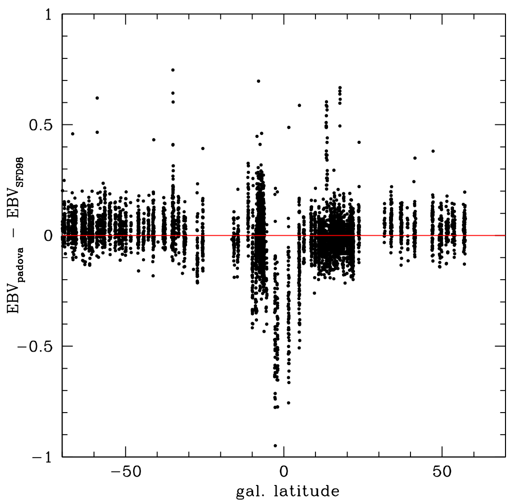

Fig. 7. Difference of E(B-V) to E(B-V) from SDF98 vs. Galactic latitude

sequences in the J vs $(J - K)$ plane. We note, however, that the effect of T_{eff} offsets rarely exceeds 10%.

Figure 2 shows the difference between the GES T_{eff} and $\log g$ and the projected value on the Padova isochrones as a function of $\sigma_{T_{eff}}$ and $\sigma_{\log g}$ (the internal GES parameter dispersions resulting from the three individual nodes, see Sect. 2). It shows that when the internal GES parameter dispersions are large, then the absolute differences between the projected T_{eff} and $\log g$ and the recommended GES ones also increase. In general, this indicates that for those few stars, the recommended parameters do not lie on top of theoretical isochrones and that offsets are performed during the projection. Given the trends illustrated in Fig. 3, we will use for our analysis only the targets with $\sigma_{T_{eff}} < 300$ K and $\sigma_{\log g} < 0.3$ dex, resulting to a total of 5603 stars.

3.1. Effect of the stellar isochrone libraries

The choice of the stellar atmosphere models used to produce the isochrones affect the derived extinctions and distances. In what follows, we compare the extinction and distance values derived from the same pipeline (see Sect. 3 and Kordopatis et al. 2011b) using alternatively the Padova and Yonsei-Yale models. We recall that Schultheis et al. (2014b) have shown that there are only small differences in the derived extinction and distances between the Padova isochrones and the corresponding Basel3.1 model library (Lejeune et al. 1997) for K/M giants observed by APOGEE. Here we want to demonstrate the importance of the chosen model library for our GES sample covering a much larger T_{eff} and $\log g$ range compared to APOGEE.

Figure 3 compares the Padova and Yonsei-Yale libraries for different combinations of ages and metallicities. One can see that the differences between the two libraries increase with decreasing metallicity. These differences concern the positions of the turn-off and the giant branch, in the sense that YY has an offset towards cooler temperatures, i.e. towards redder colours. However, the known age-colour (or age-metallicity) degeneracy (e.g. Bergemann et al. 2014, Worthey 1994) makes that the YY and the Padova models can partly overlap at a given metallicity when selecting younger YY isochrones. Since our procedure projects the observed T_{eff}, $\log g$ and [M/H] on all the ages of a set of isochrones (see above), the differences in the derived magnitudes will therefore be smaller for most types of stars than what is suggested by a simple one-to-one comparison between the isochrones. However, for the stars at the boundaries of the libraries (e.g. the hotter stars and the more metal-poor giants), the differences are expected to be the largest, due to the described offset. Finally, we also investigated the effect on the shape of the isochrones (and therefore on the derived absolute magnitudes) of atmospheric models with different $\alpha-$enhancements. The dashed and plain lines in Fig. 3, obtained for the YY isochrones, indicate only a very small effect in the T_{eff} vs. log g and J vs (J–Ks) diagram. We conclude, in agreement with other studies (e.g. Breddels et al. 2010; Zwitter et al. 2010), that the adopted $\alpha-$enhancement level of the isochrones is not affecting significantly the final distance estimations.

Figure 4 shows the comparison of the derived extinctions (left panel) and distances (right panel). It is obvious from this comparison that the YY E(B–V) values are systematically smaller than the Padova ones. In agreement with what has been stated in the previous paragraph, this means that the intrinsic colours from the YY models are redder than the Padova ones. The effect in E(B–V) can reach up to 0.2 mag showing that the choice of a certain stellar library is essential for the extinction determination. If one transforms this into distances (see right panel of Fig.4), the distances from the YY isochrones are systematically larger, especially for $d < 3$ kpc. We traced these differences as function of the stellar parameters, T_{eff}, $\log g$ and [M/H] and could identify that those arise mainly for dwarf stars ($\log g > 4$) with $5500 < T_{eff} < 6500$ K. This is consistent with Fig. 3 where the Padova isochrones predict bluer J–K colours. On the other hand, YY underestimate distances for cool giant stars with $\log g < 3$ and $4000 < T_{eff} < 5000$ K. Finally, the difference between Padova and YY increases for the most metal-poor stars ([M/H] < -1 dex). All the above discrepancies indicate important differences in the stellar atmosphere models between Padova and YY. For the majority of our objects, the differences between the two stellar libraries are within 20% (right panel of Fig. 4). In the following Section 4, we will confront the derived E(B–V) values with the dust map of Schlegel et al. 1998.

4. Comparison to the 2D extinction maps: The Schlegel map

Contrary to the study of Schultheis et al. (2014b) with APOGEE where the fields were concentrated in regions of high extinction towards the Galactic Bulge, we analyse here with GES lower extinction fields at higher latitudes. We use the Schlegel et al. (1998) dust map, hereafter referred to as SFD98, as it has the same sky coverage as our GES stars. We used the conversion $E(J - K_S)/E(B - V) = 0.527$ (Rieke & Lebofsky 1985).

As already mentioned, stellar libraries can give systematically offset extinctions. Figure 5 shows the difference in E(B–V) between the SFD98 values and the ones derived with the Padova isochrones (in black), and the YY isochrones (in red). We see clearly that the Padova isochrones match better the $E(B-V)_{SFD98}$ with a mean difference of 0.009 ± 0.075 which is the typical uncertainty of our method (derived from Eq. 3). If we include low galactic latitude fields with $|b| < 10°$, the dispersion increases to 0.18 mag where it is suspected that SFD98 overestimates extinction (Schlafly et al. 2014). Schlafly & Finkbeiner (2011) measured the dust reddening using the colors of stars derived from stellar parameters from the SDSS. Their uncertainty is in the order of 30 mmag for high latitude fields and $E(B-V) < 0.04$. Our larger dispersion is due to the lower galactic latitude fields of the GES fields. The YY isochrones systematically overestimate $E(B - V)_{SFD98}$ by 0.065 mag. For the remaining of our analysis, we decided to use the Padova isochrones, as they match better the SFD98 values.

Figure 6 shows the comparison between $E(B - V)_{Padova}$ and $E(B - V)_{SFD98}$. While there is no shift in the derived E(B-V), a large scatter is seen, especially for $E(B - V)_{SFD98} > 0.5$ where the SFD98 values are higher than $E(B - V)_{Padova}$. Our results are in agreement with those of Schlafly et al. (2014) where they compared their map based on PAN-STARRS photometry with the Schlegel map. They find systematically higher E(B–V) of SFD98 for $E(B-V)_{SFD98} > 0.3$. The Planck dust map at 353 GHz show a similar behaviour (see Schlafly et al. 2014) indicating that for higher E(B–V) the far-infrared modelling of the dust shows some systematical offsets. A revision of these models is therefore needed.

We now assess the existence of biases as a function of T_{eff}, $\log g$ and [M/H] between our derived extinction and the SFD98 map. Figure 8 displays a small trend of the differences in E(B–V) towards higher temperatures ($T_{eff} > 6000$ K) in the sense that SFD98 gets higher E(B–V) with respect to $E(B - V)_{Padova}$. For cooler temperatures ($T_{eff} < 4500$ K) SFD98 predicts higher E(B–V) than $E(B - V)_{Padova}$. While for the range

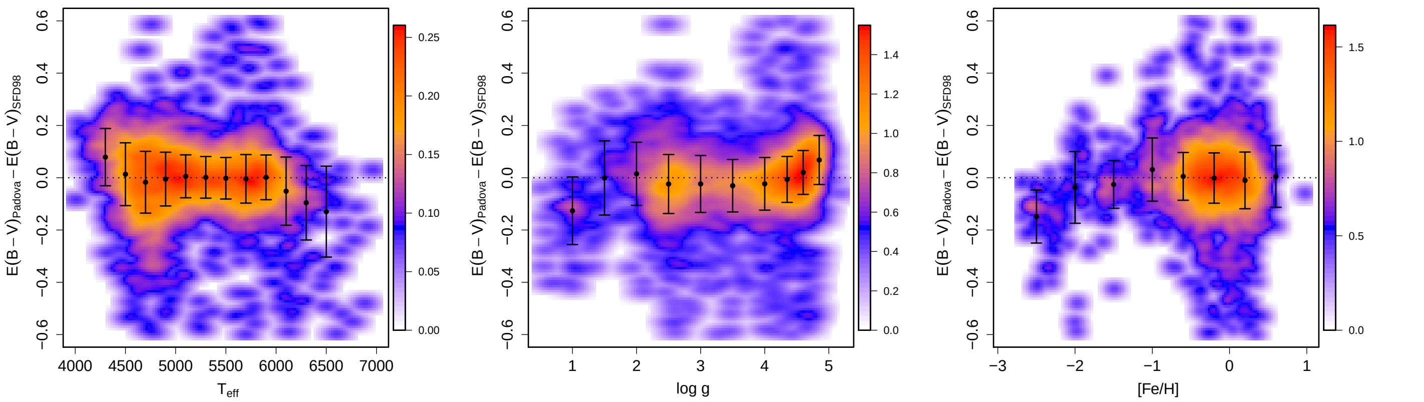

Fig. 8. Difference in E(B–V) to SFD98 as a function of (a) $T_{\rm eff}$, (b) log g, and (c) [Fe/H] for high galactic latitude stars (|b| > 10°).The median value is indicated by black dots together with the standard deviation

1.5 < log g < 4.5 no trend is visible, giants with log g < 1.5 have a slightly overestimated extinction compared to $E(B-V)_{\rm SFD98}$. Interestingly, our E(J–K) estimation for dwarf stars with log g > 4.5 and 4000 < $T_{\rm eff}$ < 6000 K is slightly offset towards higher values with respect to $E(J-K)_{\rm SFD98}$.

The derived extinction depends on the corresponding matched colour of the isochrone as well as of the stellar parameters, the surface gravity being a particularly sensitive parameter. Indeed, systematic offsets of 0.2 dex can significantly shift the extinctions and distances (see Sect. 3). This effects mainly giant stars while GES has mostly dwarf stars (see Fig. 2 of Recio-Blanco et al. 2014a).

5. Comparison to three-dimensional maps

In this section, we compare our 3D extinction distributions with the model of Drimmel et al. (2003) and the map of Chen et al. (2014b). The Drimmel et al. (2003) model is based on the far and near-IR data fits of the dust distribution made by Drimmel & Spergel (2001) from the COBE/DIRBE instrument. The spatial resolution of this map is approximately 21′× 21′, we however recall that the Drimmel et al. model does not include features related to the Galactic bar nor the nuclear disk, resulting to systematic overestimates of the extinction towards the Galactic Bulge, (see Schultheis et al. 2014b, for further details).

As far as the Chen et al. (2014b) 3D map is concerned, we found only a limited spatial overlap with six GES fields. Chen et al. (2014b) combined optical photometry (g, r, i) with 2MASS (J, H, K) and WISE (W1, W2) photometry and used the method of Berry et al. (2012) to trace the stellar locus in a multi-dimensional colour space. The constructed 3D map is over roughly 6000 sq. degree towards the Galactic anticenter region, with an angular resolution varying between 3–9′.

Figure 9 displays for different heights above the Galactic plane, the A_K extinctions measured from the GES targets. The illustration is made in a Cartesian Galactocentric (X,Y) frame, with the Sun located at 8 kpc from the centre. Superimposed in the panel representing the closest distance from the plane, is the illustration of our Galaxy produced by Robert Hurt based on the results of the Spitzer Infrared Space telescope (R. Benjamin). Compared to the APOGEE targets, where the majority of them are located at distances larger than about 6 kpc, the GES targets probe a volume much closer to the Sun with typical distances d ∼ 2 − 3 kpc. From Fig. 9, one can see that GES also contains a line-of-sight in the direction of the Galactic bar (l = 28°, b = −3°), which shows a higher concentration of dust. According to Schultheis et al. (2014b) this is associated to a dust lane in front of the bar. Clearly visible is also the increased dust amount associated with the Perseus spiral arm, the Sagittarius arm and the Scutum-Centaurus arm. Most of the low extinction is situated in the first few kpc around the Sun's position.

Figures 10 and 11 show the 3D extinction for a few selected lines of sight and compare our results with the ones of Drimmel et al. and Chen et al. We present in the online table (see A.1) additional lines of sights of 3D extinction for different GES fields. Below we describe a few trends:

– Contrary to the APOGEE data, GES samples the first few kpc at higher spatial resolution in distance. In general one sees a steep rise in A_V (see Fig. 10).
– The Drimmel et al. model underestimates A_V systematically for high Galactic latitudes (l > |50|). The Chen et al. map predicts a steeper increase in A_V for the first kpc than Drimmel et al. which seem to be in better agreement with the GES data (see Fig. 11).
– For most of the lines of sight, we see a steep rise in A_V followed by a flattening afterwards which is qualitatively described by the Drimmel model. Due the low absolute extinction values, the errors in the derived extinction and distances become significant for distances larger than 4 kpc.
– Puspitarini et al. (2014) studied the DIBS of 225 GES stars in five fields and found a good correlation between the DIB strength and the extinction. We have one field in common which is the "COROT-ANTICENTER" field (see upper left panel of Fig.11, located at (l, b) = (+212.87, −2.04)°. They found a steep increase in extinction up to 1 kpc, a plateau between 1 to 2.5 kpc and a second increase beyond 2.5 kpc (see their Fig. 6). We confirm the steep increase in A_V between 0 and 1.5 kpc with a flattening starting at around 2 kpc. There are too few data points to see their second increase in A_V.
– The GES fields located at (l, b) = (+38.30, −6.51)°, (l, b) = (+14.60, +21.85)°, and the field at (l, b) = (+147.13, −2.04)° span the full distance range and follow the A_V vs. distance relation predicted by Drimmel et al.

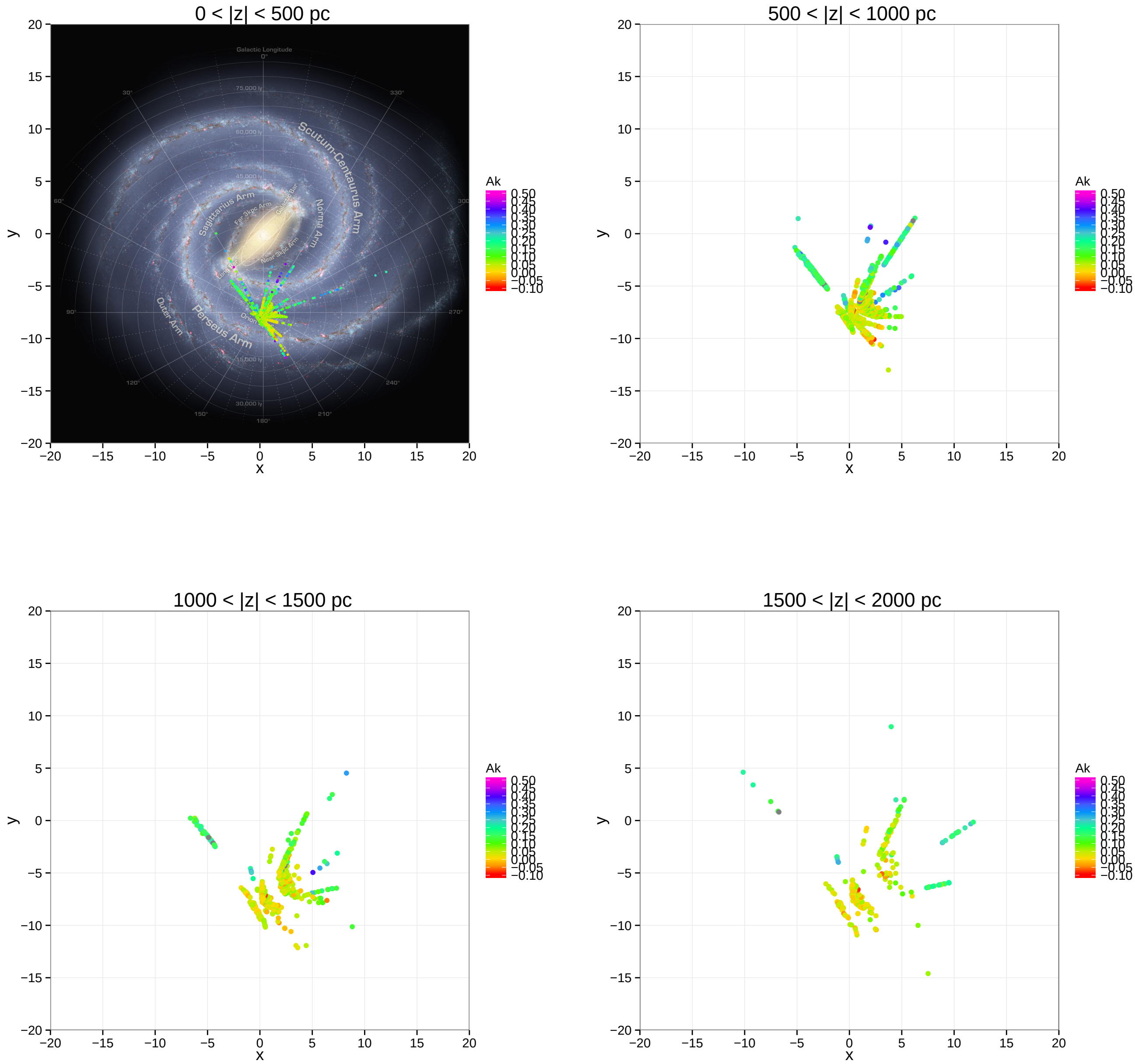

Fig. 9. Extinction in the (X,Y) plane for different heights above the galactic plane. On the left upper plot an illustration of our Galaxy produced by R. Hurt is superimposed.

– The GES data seem to confirm the general shape of the 3D extinction with a steep rise in A_V for distances up to 4 kpc and a flattening which occurs at shorter distances compared to the values found with the APOGEE sample of Schultheis et al. (2014b).

With the future data releases of GES in the coming years, we will be able to systematically trace the distance vs. A_V behaviour systematically allowing to compare qualitatively spectroscopically derived extinction with 3D dust models. The combination of both GES and APOGEE data tracing the low-extinction fields in the Visible as well as the high-obscured fields in the Infrared will be clearly a goal for the future for tracing 3D extinction

6. Interstellar extinction law

Using the extinctions derived by the GES sample, we now investigate the universality of the extinction law, as a function of the position on the sky and the stellar environment. Using APOGEE red clump stars, Wang & Jiang (2014) recently found a constant power law with alpha = 1.95 yielding $A_J/A_{K_S} = 2.88$. They used stars with $3500 < T_{\rm eff} < 4800$ K, $\log g < 3$ and [Fe/H] > -1.0 dex. On the other hand, Yuan et al. (2013) combined SDSS, GALEX, 2MASS and WIDE photometry to determine reddening coefficients from the far UV to the near and mid-IR by using the SDSS spectroscopic archive. They concluded that their newly derived extinction coefficients differ slightly but favour

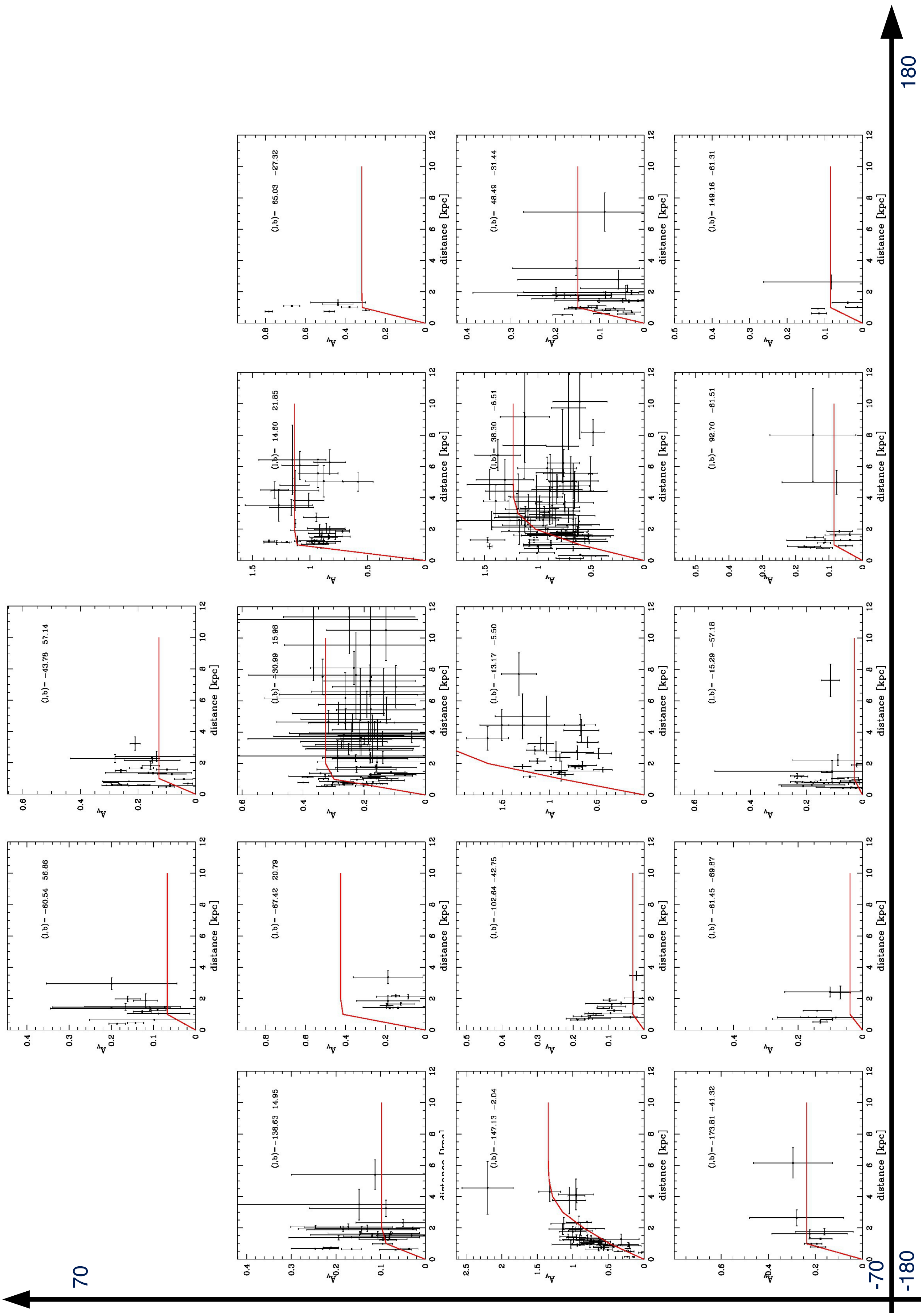

Fig. 10. Extinction vs distance for different lines of sight. The x-axis and y-axis give approximate the location in Galactic coordinates. The Drimmel et al. (2003) model is superimposed in red

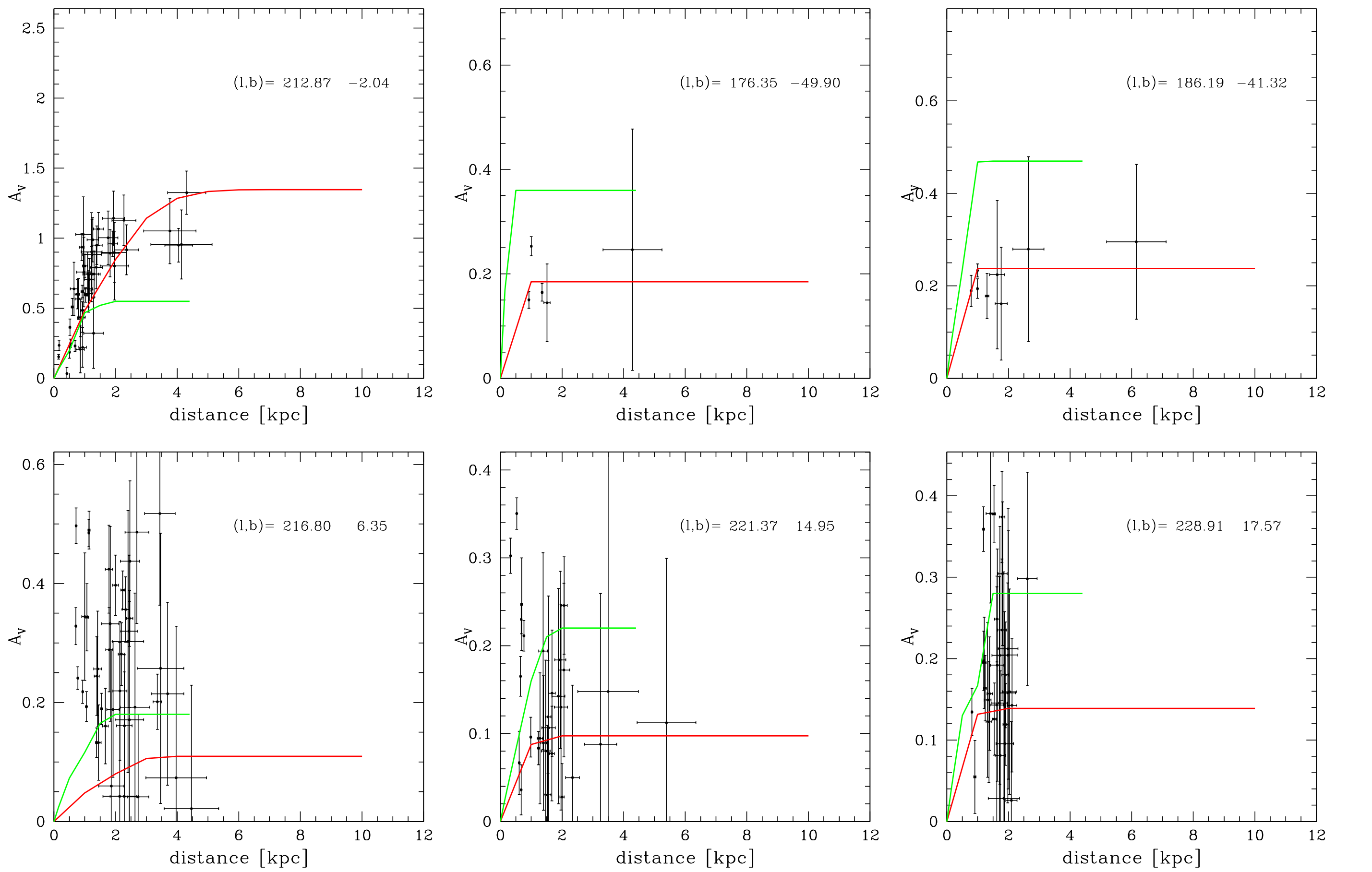

Fig. 11. Extinction vs distance for different lines of sight where. In red the 3D extinction model of Drimmel et al. (2003) is superimposed while in green the 3D-model of Chen et al. (2013).

the R(V)=3.1 Fitzpatrick reddening law (Fitzpatrick 1999) over the Cardelli et al. (Cardelli et al. 1989) and the O'Donnell et al. (O'Donnell 1994) reddening laws.

Here we perform a similar study and aim to push the analysis to the investigation of the systematic dependencies of the extinction law as a function of the stellar parameters ($T_{\rm eff}$, log g, [Fe/H]). Besides the near-IR photometry we use SDSS photometry in the filters u,g,r,i,z giving us the the possibility to trace simultaneously the extinction law in the optical and the IR. For every band, the colour excess is simply the difference between the intrinsic colour derived from the isochrone matching method and the observed colour. Figure 12 shows the linear fit results of the different colour excess similar as done by Yuan et al. (2013) and Wang & Jiang (2014). We forced the intercept to be zero as done as in Wang & Jiang (2014). Figure 12 displays our best fitting results and Table 2 gives the fitting parameters as well as the comparison to Yuan et al. (2013) and Fitzpatrick (1999) and Cardelli et al. (1989).

The extinction coefficients we derive agree within 10% with Yuan et al. (2013) except for u-g where we find a value closer to the Fitzpatrick extinction law. The u–g dispersion we measure is higher than for other colours with some outliers not following the linear relation between E(u-g) and E(g-r) (see Fig. 12). The observed r.m.s scatter is ~ 0.1 mag in the u-band which is in agreement with the estimated uncertainties.

Up to now, most of the studies have mainly been concentrating on deriving interstellar extinction coefficients using a spe-

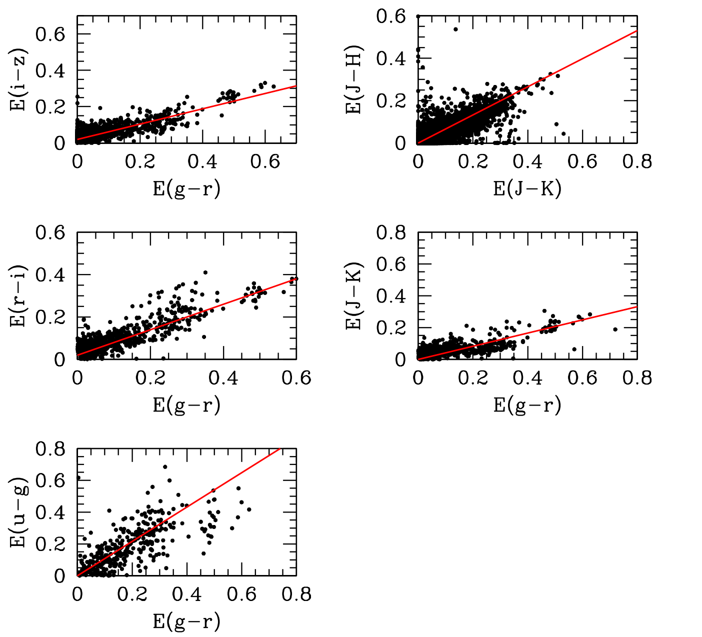

Fig. 12. Relation between different colour excesses. The red line denotes the best linear fitting.

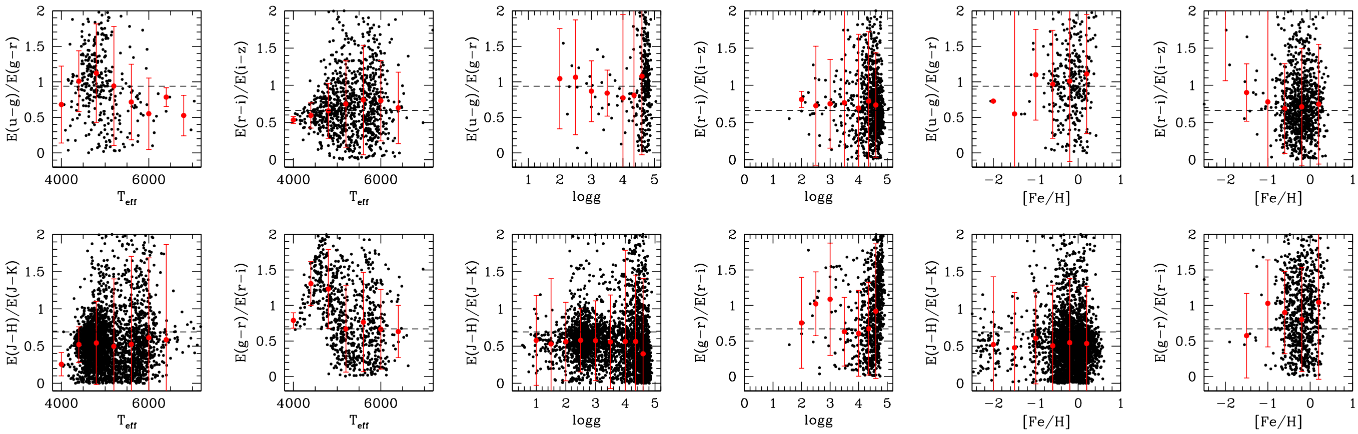

Fig. 13. Extinction coefficients as a function of T_{eff}, log g and [M/H].

Table 2. Derived slopes of the colour-excesses

Colour	This work	Yuan et al.	Fitzpatrick	Cardelli
u – g[a]	0.94 ±0.03	1.08 ±0.010	0.945	0.984
r – i[a]	0.64 ±0.02	0.60 ±0.010	0.582	0.557
i – z[a]	0.48 ±0.01	0.43 ±0.004	0.426	0.496
J – K[a]	0.41 ±0.01	0.414 ±0.01	0.411	0.466
J – H[b]	0.65 ±0.02	0.63 ±0.01	–	–

[a] derived by fitting versus $E(g - r)$ diagram
[b] derived by fitting versus $E(J - K)$ diagram

cific population or a mixture of stars with different stellar parameters. However, as first suggested by Wildey (1963), other factors such as the stellar abundance may affect the interstellar extinction. In particular, Grebel & Roberts (1995) showed that the colour dependence of interstellar extinction is a complicated function of the temperature, luminosity, and metallicity of the stellar probe. Even the ratio of total to selective extinction depends on these parameters and R_V can, according to their model, vary more than 10% between a star having T_{eff} = 3500 K and another one having T_{eff} = 10 000 K. Figure 13 shows the extinction coefficient (defined as the ratio of two colour excesses) as a function of T_{eff} and log g. It is clear from Fig. 13 that our method does not have the required accuracy to detect variations at the level of 10% as predicted by the theoretical models of Grebel & Roberts (1995). However, within the accuracy of our procedure, large scale variations of the different extinction coefficients as a function of T_{eff}, log g or [M/H] are not detected. We note, on the other hand, that the dispersion increases for higher log g.

Due to the limited spatial overlap between SDSS and the GES, only a small number of our GES sources have SDSS ugriz photometry. For the targets for which we have SDSS photometry, the E(g–r)/E(r–i) ratio is overestimated for cool giant stars with T_{eff} < 5000 K and log g < 3.5. Within the large dispersion of our method we do not note any hint of a dependence of the extinction coefficient to the Galactic environment, i.e. the metallicity of the stars. However, we lack of stars with [M/H] < −1 dex and small-scale variations cannot not be excluded by our method. Striking is the nearly flat extinction coefficient in the near-IR (e.g. E(J − H)/E(J − K)) plane with no variation as a function of the stellar parameters. Within the errors of our method, our work does not show that there is any dependence of the interstellar extinction coefficient on the atmospheric parameters of the stars. This suggests, that extinction maps derived from mean colours of stars such as the RJCE method (Majewski et al. 2011) or the colour-excesses of stars (Lada et al. 1994, Gonzalez et al. 2012) can be generally used, assuming a constant extinction coefficient which does not depend on the stellar parameter. We fitted the E(J–H) vs. E(J–K) diagram in the same way as Wang & Jiang (2014). Our value E(J − H) = 0.651 ± 0.009 × E(J − Ks) is slightly higher than the one of Wang & Jiang (2014) who measured E(J − H) = 0.641 ± 0.001 × E(J − Ks), resulting to a power law index of α = 2.12 and A_J/A_{Ks} = 3.15 (assuming λ_{eff} = 1.25 μm, 1.65 μm, 2.15 μm for the J,H,K_S bands). Our power law index is similar to that of Stead & Hoare (2009) with α = 2.14 or Fritz et al. (2011) with α = 2.11.

Finally, we investigated the variation of the extinction coefficient along different lines of sight. Zasowski et al. (2009) and Gao et al. (2009) suggested strong variations in the extinction law in the mid-IR as a function of Galactic longitude or angle from the Galactic Center. Strong variation of the extinction law as a function of the Galactic latitude was also found by Chen et al. (2013) in the Galactic Bulge. Zasowski et al. (2009) suggested the existence of strong longitudinal variations in the infrared extinction law where the slopes increase as the wavelength increase (see their Fig. 5) resulting in a steeper extinction curve in the outer Galaxy. Gao et al. (2009) identified small variations of the mid-IR extinction law with the location of the spiral arms. Figure 14 shows the extinction coefficient E(J–H)/E(J–K) as a function of the angle from the Galactic Center (see Fig. 14). Note that contrary to APOGEE, GES probes different regions of the Galaxy and avoids especially the galactic plane where interstellar extinction is very high.

Within the dispersion of our method, we do not find evidence for any trend of the variation of E(J–H)/E(J–K) with the angle from the Galactic Center nor with Galactocentric distance in agreement with the extinction coefficients in the SDSS bands. This suggests that the extinction law in the SDSS ugriz bands and the near-IR JHKs bands is uniform, confirming the result of Wang & Jiang (2014) obtained with APOGEE red clump stars.

7. Conclusions

We used data from the GES survey, together with accurate stellar parameters (T_{eff}, log g, [M/H]) to trace 3D interstellar extinction in intermediate and high-latitude regions of our Galaxy. We discuss the influence of different stellar isochrones (Yonsei-Yale and Padova) on the derived 3D extinction and compare our re-

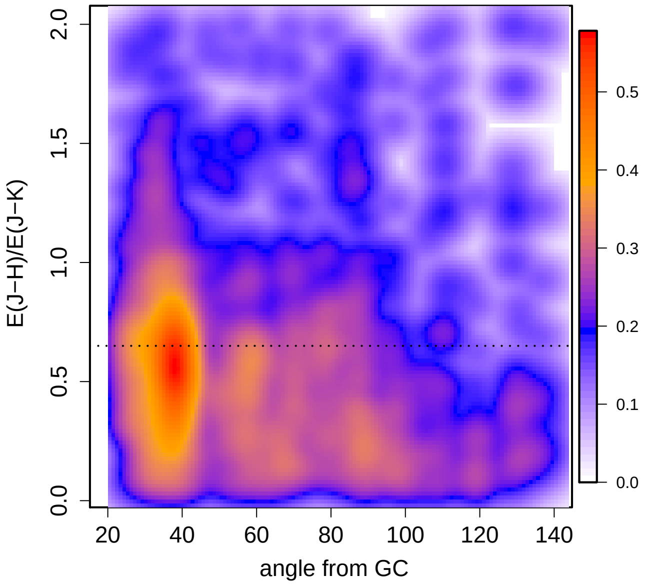

Fig. 14. Density plot of E(J–H)/E(J–K) vs. angle from the Galactic Center. The dashed blanck line gives the mean of our derived extinction coefficient.

sults with the SFD98 dust maps. We find on average good agreement with a mean difference of $\Delta E(B-V) = 0.009 \pm 0.075$, with the dispersion getting larger when including low galactic latitude regions (|b| < 10°). For larger E(B − V) > 0.5 SFD98 gets higher extinction compared to our estimation $E(B-V)_{Padova}$.

We compared our 3D interstellar dust maps with those of Drimmel et al. (2003) and Chen et al. (2014b). The GES data confirm the steep rise in A_V for distances between 0 and 4 kpc with a flattening of the extinction at larger distances. We studied the influence of the stellar parameters on the extinction coefficients in the optical (SDSS-bands) and the near-IR (JHKs). We do not detect any significant dependence of the extinction coefficient with stellar parameters indicating that a constant extinction coefficient can be assumed. Within the precision of our method, we do not find any evidence for the variation of the extinction coefficients with the angle from the Galactic centre or Galactocentric distance. We note, however, that our method does not allow to trace small-scale variations of the extinction coefficient. This suggests a uniform extinction-law, as found in Wang & Jiang (2014). With the future data releases of GES in the coming years, we will be able to trace the distance vs. A_V behaviour, systematically allowing to compare qualitatively spectroscopically derived extinction with 3D dust models

Acknowledgements. We want to thank the anonymous referee for her/his extremly useful comments. Based on data products from observations made with ESO Telescopes at the La Silla Paranal Observatory under programme ID 188.B-3002. This work was partly supported by the European Union FP7 programme through ERC grant number 320360 and by the Leverhulme Trust through grant RPG-2012-541. We acknowledge the support from INAF and Ministero dell' Istruzione, dell' Università' e della Ricerca (MIUR) in the form of the grant "Premiale VLT 2012". The results presented here benefit from discussions held during the Gaia-ESO workshops and conferences supported by the ESF (European Science Foundation) through the GREAT Research Network Programme. We want to thank C. Bailer-Jones, C. Babusiaux for extremly useful comments. M. Schultheis, A. Recio-Blanco, P. de Laverny et V. Hill acknowledge the support of the "Programme National de Cosmologie et Galaxies" (PNCG) of CNRS/INSU, France. TB is funded by grant no. 621-2009- 3911 from the Swedish Research Council.

References

Allende Prieto, C., Beers, T. C., Wilhelm, R., et al. 2006, ApJ, 636, 804
Bailer-Jones, C. A. L. 2011, MNRAS, 411, 435
Bailer-Jones, C. A. L., Andrae, R., Arcay, B., et al. 2013, A&A, 559, A74
Bergemann, M., Ruchti, G. R., Serenelli, A., et al. 2014, A&A, 565, A89
Berry, M., Ivezić, Ž., Sesar, B., et al. 2012, ApJ, 757, 166
Boulanger, F. 2007, in IAU Symposium, Vol. 237, IAU Symposium, ed. B. G. Elmegreen & J. Palous, 47–52
Breddels, M. A., Smith, M. C., Helmi, A., et al. 2010, A&A, 511, A90
Bressan, A., Marigo, P., Girardi, L., et al. 2012, MNRAS
Cardelli, J. A., Clayton, G. C., & Mathis, J. S. 1989, ApJ, 345, 245
Carpenter, J. M., Hillenbrand, L. A., & Skrutskie, M. F. 2001, AJ, 121, 3160
Chabrier, G. 2003, ApJ, 586, L133
Chen, B.-Q., Liu, X.-W., Yuan, H.-B., et al. 2014a, MNRAS, 443, 1192
Chen, B.-Q., Liu, X.-W., Yuan, H.-B., et al. 2014b, MNRAS, 443, 1192
Chen, B. Q., Schultheis, M., Jiang, B. W., et al. 2013, A&A, 550, A42
Demarque, P., Woo, J.-H., Kim, Y.-C., & Yi, S. K. 2004, ApJS, 155, 667
Drimmel, R., Cabrera-Lavers, A., & López-Corredoira, M. 2003, A&A, 409, 205
Drimmel, R. & Spergel, D. N. 2001, ApJ, 556, 181
Fitzpatrick, E. L. 1999, PASP, 111, 63
Fritz, T. K., Gillessen, S., Dodds-Eden, K., et al. 2011, ApJ, 737, 73
Gao, J., Jiang, B. W., & Li, A. 2009, ApJ, 707, 89
Gazzano, J.-C., Kordopatis, G., Deleuil, M., et al. 2013, A&A, 550, A125
Gilmore, G., Randich, S., Asplund, M., et al. 2012, The Messenger, 147, 25
Gonzalez, O. A., Rejkuba, M., Zoccali, M., Valenti, E., & Minniti, D. 2011, A&A, 534, A3
Gonzalez, O. A., Rejkuba, M., Zoccali, M., et al. 2012, A&A, 543, A13
Grebel, E. K. & Roberts, W. J. 1995, A&AS, 109, 293
Green, G. M., Schlafly, E. F., Finkbeiner, D. P., et al. 2014, ApJ, 783, 114
Hanson, R. J. & Bailer-Jones, C. A. L. 2014, MNRAS, 438, 2938
Kordopatis, G., Hill, V., Irwin, M., et al. 2013, A&A, 555, A12
Kordopatis, G., Recio-Blanco, A., de Laverny, P., et al. 2011a, A&A, 535, A106
Kordopatis, G., Recio-Blanco, A., de Laverny, P., et al. 2011b, A&A, 535, A107
Lada, C. J., Lada, E. A., Clemens, D. P., & Bally, J. 1994, ApJ, 429, 694
Lallement, R., Vergely, J.-L., Valette, B., et al. 2014, A&A, 561, A91
Lejeune, T., Cuisinier, F., & Buser, R. 1997, A&AS, 125, 229
Lejeune, T., Cuisinier, F., & Buser, R. 1998, A&AS, 130, 65
Majewski, S. R., Zasowski, G., & Nidever, D. L. 2011, ApJ, 739, 25
Marigo, P. 1998, A&A, 340, 463
Marshall, D. J., Robin, A. C., Reylé, C., Schultheis, M., & Picaud, S. 2006, A&A, 453, 635
Minniti, D., Lucas, P. W., Emerson, J. P., et al. 2010, New A, 15, 433
Nataf, D. M., Gould, A., Fouqué, P., et al. 2013, ApJ, 769, 88
Nidever, D. L., Zasowski, G., & Majewski, S. R. 2012, ApJS, 201, 35
Nishiyama, S., Tamura, M., Hatano, H., et al. 2009, ApJ, 696, 1407
O'Donnell, J. E. 1994, ApJ, 422, 158
Puspitarini, L., Lallement, R., Babusiaux, C., et al. 2014, ArXiv e-prints
Recio-Blanco, A., Bijaoui, A., & de Laverny, P. 2006, MNRAS, 370, 141
Recio-Blanco, A., de Laverny, P., Kordopatis, G., et al. 2014a, A&A, 567, A5
Recio-Blanco, A., de Laverny, P., Kordopatis, G., et al. 2014b, ArXiv e-prints
Rieke, G. H. & Lebofsky, M. J. 1985, ApJ, 288, 618
Robin, A. C., Reylé, C., Derrière, S., & Picaud, S. 2003, A&A, 409, 523
Sale, S. E. 2012, MNRAS, 427, 2119
Sale, S. E., Drew, J. E., Barentsen, G., et al. 2014, MNRAS, 443, 2907
Schlafly, E. F. & Finkbeiner, D. P. 2011, ApJ, 737, 103
Schlafly, E. F., Finkbeiner, D. P., Schlegel, D. J., et al. 2010, ApJ, 725, 1175
Schlafly, E. F., Green, G., Finkbeiner, D. P., et al. 2014, ApJ, 789, 15
Schlegel, D. J., Finkbeiner, D. P., & Davis, M. 1998, ApJ, 500, 525
Schultheis, M., Chen, B. Q., Jiang, B. W., et al. 2014a, A&A, 566, A120
Schultheis, M., Zasowski, G., Allende Prieto, C., et al. 2014b, AJ, 148, 24
Stead, J. J. & Hoare, M. G. 2009, MNRAS, 400, 731
Valenti, J. A. & Piskunov, N. 1996, A&AS, 118, 595
Wang, S. & Jiang, B. W. 2014, ApJ, 788, L12
Wildey, R. L. 1963, AJ, 68, 190
Worthey, G. 1994, ApJS, 95, 107
Yuan, H. B., Liu, X. W., & Xiang, M. S. 2013, MNRAS, 430, 2188
Zasowski, G., Majewski, S. R., Indebetouw, R., et al. 2009, ApJ, 707, 510
Zwitter, T., Matijevič, G., Breddels, M. A., et al. 2010, A&A, 522, A54

Appendix A: 3D extinction along different lines of sights of GES

Fig. A.1. 3D extinctions for GES lines of sight for GES field. The red straight line gives the corresponding model of Drimmel et al. (2003)

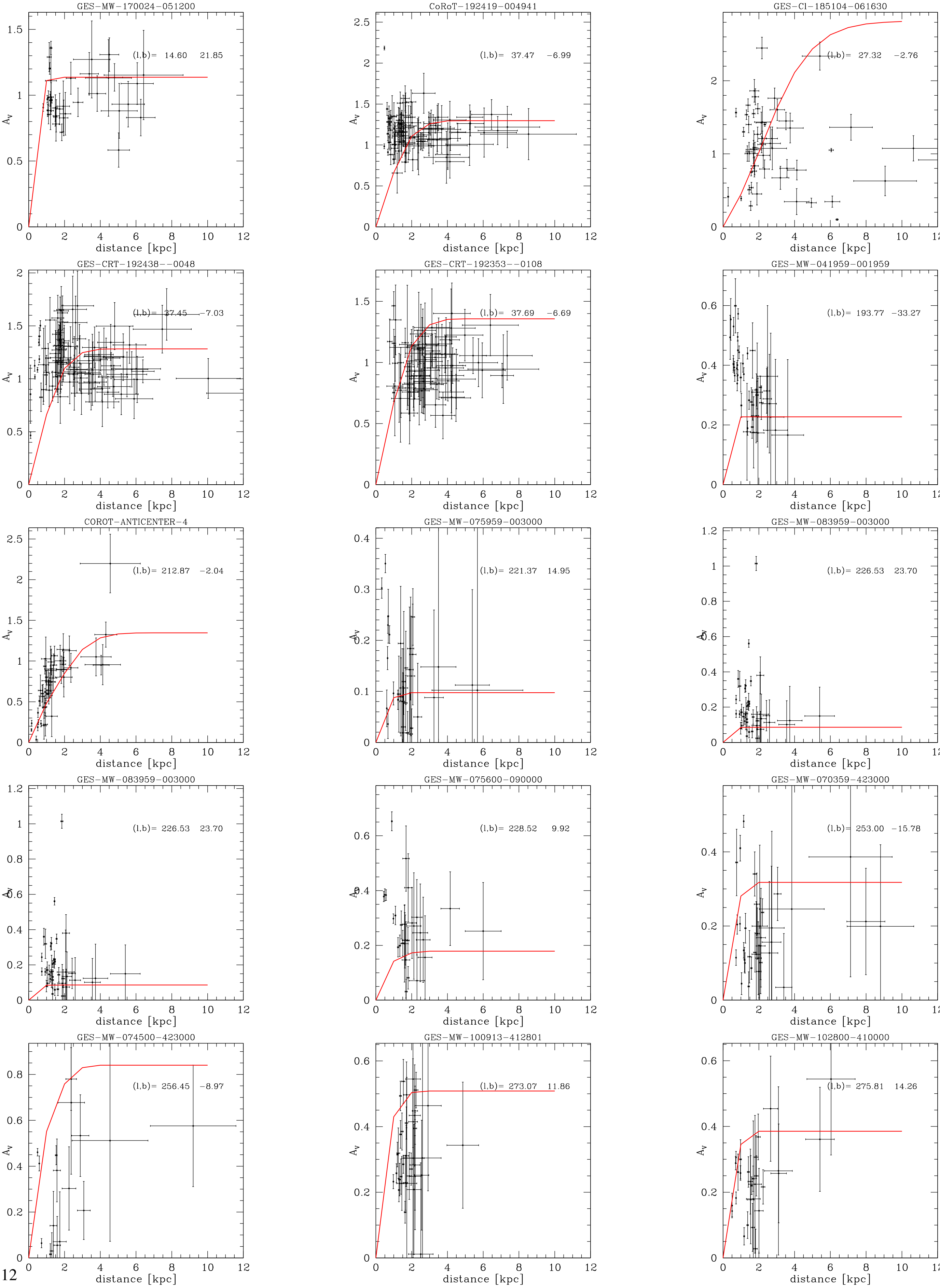

Fig. A.2. 3D extinctions for GES lines of sight for GES field (continued)